Rapid Sintering of Anisotropic, Nanograined Nd-Fe-B by Flash-Spark Plasma Sintering

Elinor Castle[a*], Richard Sheridan[b], Salvatore Grasso[a], Allan Walton[b], Mike Reece[a]

a) Queen Mary, University of London, Mile End Road, London, E1 4NS, UK
b) University of Birmingham, Edgbaston, Birmingham, West Midlands, B15 2TT, UK
*Corresponding author: Room 2.08 Nanoforce, Joseph Priestley Building, Queen Mary, University of London, Mile End Road, London, E1 4NS. UK. E-mail: e.g.castle@qmul.ac.uk

Abstract

A Spark Plasma Sintering (SPS) furnace was used to Flash-Sinter (FS) Nd-Fe-Dy-Co-B-Ga melt spun permanent magnetic material. During the 10 second "Flash" process (heating rate 2660 K min^{-1}), sample sintering (to theoretical density) and deformation (54 % height reduction) occurred. This produced texturing and significant magnetic anisotropy, comparable to conventional die-upset magnets; yet with much greater coercivities (>1600 kA m^{-1}) due to the nanoscale characteristics of the plate-like sintered grains. These preliminary results suggest that Flash-SPS could provide a new processing route for the mass production of highly anisotropic, nanocrystalline magnetic materials with high coercivity.

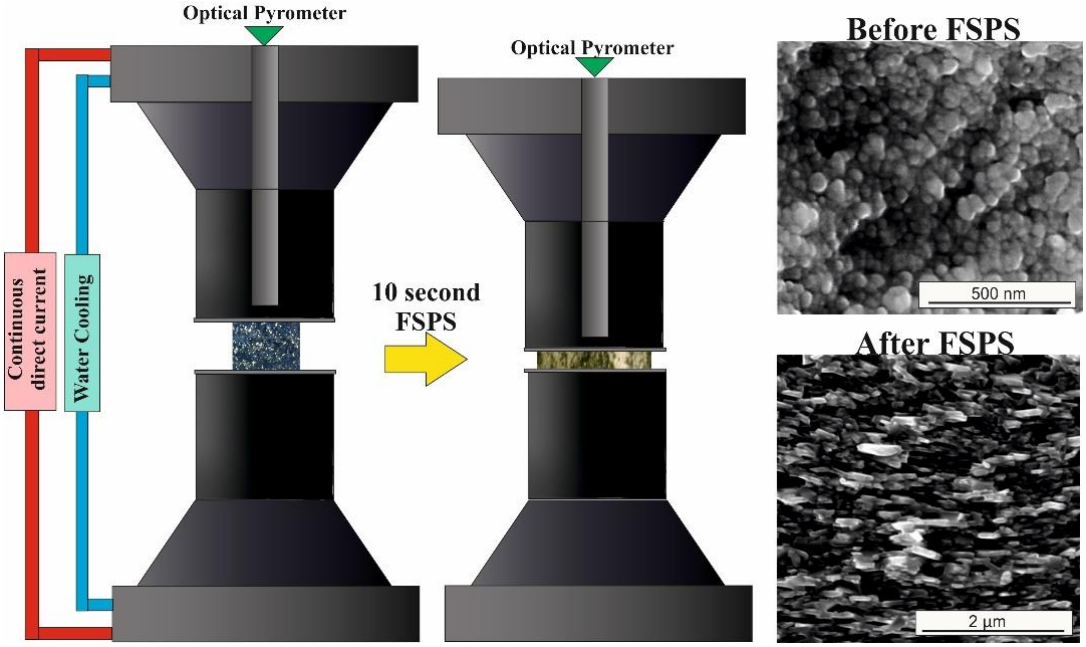

Highlights:

- **Novel 'Flash Spark Plasma Sintering' technique was applied to melt-spun Nd-Fe-B**
- **Extremely rapid deformation (<3.6 s^{-1}) and heating (2660 K min^{-1}) observed**
- **Anisotropic, nanostructured, high coercivity (1600 kA m^{-1}) material produced**
- **'FSPS' is a promising technique for efficient production of anisotropic Nd-Fe-B**

Keywords: Magnetic anisotropy; high-speed deformation; spark plasma sintering; hard magnetic materials; flash sintering.

1.1 Introduction

Significant work has been undertaken towards the goal of finding a quick and economic method for the production of anisotropic (high remanence), nanoscale (high coercivity) Nd-Fe-B-based magnetic materials for use in applications such as electrical generators, permanent magnet motors and other green energy technologies. Conventional powder metallurgy routes involve multiple process steps; including magnetic pulse-alignment and compaction of powders into anisotropic green parts, followed by long sintering treatments at high temperature (~1 hour at >1000 °C). This leads to expensive production costs and significant grain growth. Magnetic alignment has also been attempted during hot pressing in the presence of an applied magnetic field [1], however, this was largely unsuccessful.

Conventional commercial processing typically employs the use of hot deformation techniques, such as die-upset forging or back extrusion, in order to produce anisotropic material from isotropic Nd-Fe-B powders produced by rapid solidification melt spinning [2-4]. These hot deformation techniques are preceded by a hot pressing step, designed to produce fully dense, isotropic material. The hot pressing of Nd-Fe-B melt spun ribbons to produce fully dense magnets was first described by Lee et al. [2]. In order to encourage sufficient plastic flow for full densification to occur during hot pressing, Lee et al. determined that pressures of 70-210 MPa, applied at temperatures of 700-750 °C for 1-3 minutes, were required. Hot pressing can be achieved at lower temperatures (650 °C), however, extremely high pressures (300 MPa) are required in order to reach full density [4]. It was observed from the work by Lee et al. [2] that a slight preferential magnetisation direction was established parallel to the pressing direction, accompanied by equiaxial grain growth. The fully dense hot-pressed magnets were then die-upset forged at 650-750 °C to produce a height reduction of up to 50%, which yielded excellent magnetic alignment parallel to the pressing direction; with a typical remanence of ~1.2 T and coercivity ~1050 kAm^{-1}. Transmission electron microscopy showed that the die-upsetting process reduced the thickness of the melt spun ribbons and formed elongated plate-like grains by strain induced alignment.

In recent years research has focussed on the use of Electric Current Assisted Sintering (ECAS) techniques such as Spark Plasma Sintering (SPS) [5-9]. Such techniques enable isotropic, nanocrystalline, melt-spun magnetic powders to be sintered to full density in much shorter sintering times by the application of high pressures and electric fields/currents. The rapid nature of these techniques allow a very fine grain size to be maintained; resulting in high magnetic coercivity [5, 10]. However; in order to produce anisotropic, high maximum energy product $(BH)_{max}$ magnets that are competitive with the hot pressed and die upset magnets currently on the market, additional post-SPS hot deformation/die upset steps are still required in order to improve the c-axis alignment of the $Nd_2Fe_{14}B$ phase [11-14].

Recent advances in ECAS include the development of Flash Sintering (FS). FS is a densification technique that has attracted much attention since the publication of the paper of Cologna et al. (2010) [15]. In this work, it was demonstrated that their FS technique could sinter yttrium-stabilised zirconia to full density at an experimental temperature of 850 °C in a matter of seconds; a process which would usually take several hours at 1450 °C. Flash sintering occurs due to the sudden increase in electrical conductivity observed at a critical combination of temperature and applied electric field. A number of materials have now been successfully consolidated using FS, including: potassium-

niobate, $KNbO_3$ [16]; manganese cobaltite spinel, $MnCo_2O_4$ [17, 18]; silicon carbide, SiC [19]; tin dioxide, SnO_2 [20] and titania, TiO_2 [21]. However, there are some drawbacks to the currently employed FS technique. For ceramic materials of low electrical conductivity, voltage gradients of more than 100 V cm^{-1} are required to initiate the flash. As such, only a limited quantity of material (0.6g of TZ3Y in the case of Cologna et al. [15]) can be sintered, and a bone-shaped green compact must be used to maximise the power dissipation. Furthermore, this green compact must be suspended from expensive platinum wire electrodes within a furnace in order to achieve the pre-heating required.

Recently, Grasso et al. [22] demonstrated that FS can be achieved with ZrB_2 using a simple modified SPS furnace. The high electrical conductivity of ZrB_2 makes it suitable for FS in SPS (FSPS), since the voltage gradients required to produce the flash are low and SPS is a low voltage (< 10 V) technique. By removing the graphite die usually employed for SPS processing and placing the green sample in between two graphite punches, all of the applied current is forced through the sample. Using this configuration, Grasso et al. then heated samples under peak heating powers of around 25 kW for up to 35 s; subsequently achieving relative densities of up to 95 %.

During FSPS the sample is not constrained by a die; and thus deformation can occur. As such, FSPS may represent a more efficient and effective means of producing anisotropy in isotropic Nd-Fe-B powder compacts during sinter-forging. The present report describes the results of an initial investigation into the processing of Nd-Fe-B powders by FSPS. The high deformation rates, anisotropic grain growth and alignment observed in FSPS samples suggest that this technique could offer a more effective alternative to the conventional die upset methods used to fabricate high energy density magnets.

2.1 Materials and Methods

All experiments were performed under vacuum (~5 Pa) using a Spark Plasma Sintering (SPS) furnace (FCT HPD 25; FCT Systeme GmbH, Rauenstein, Germany). The temperature was monitored using an infrared pyrometer positioned at the top of the SPS system and directed through channels in the top piston and graphite tooling; such that continuous temperature measurements were taken from inside the top graphite punch at a distance of 4 mm from the sample. During each experiment, the SPS software logged data for: current, voltage and power outputs; processing time; pressure; temperature; and top piston displacement and speed (related to sample shrinkage speed). A full record of processing conditions was therefore available for post-processing analysis.

Commercial melt-spun Nd-Fe-Dy-Co-B-Ga powder (“MQU-G”), containing 26.4 wt.% Nd and 3.72 wt.% Dy, was supplied by Molycorp Magnequench. The raw, flake-like powder was imaged using SEM Secondary Electron imaging (FEI Inspect™-F SEM) and the resulting images used for grain size and aspect ratio analysis. Here the lengths and widths of 225 grains were measured across the thickness of several powder flakes. Nearly-equiaxed grains were observed throughout the powder; exhibiting an average length of 55 ±14 nm, width of 47 ±13 nm, and aspect ratio of 1.19 ±0.19.

Grain size and aspect ratio analysis was also performed on all of the sintered samples after fracturing them parallel to the pressing direction. Measurements were taken near the top, middle and bottom

of each sintered sample (along the pressing direction) in order to obtain a more accurate representation of the whole microstructure.

One sample was fabricated using standard SPS processing conditions for comparison with the FSPS processed samples. Here, 20 g of powder was poured into a 20 mm diameter graphite die & punch set lined with graphite foil, cold-pressed to 7 MPa and sintered at 923 K for 10 min under 50 MPa uniaxial pressure. These processing conditions were chosen based on previous work, wherein SPS parameters were optimised to produce near-theoretical density while minimising grain growth; with an average measured grain length of 171 ± 140 nm, and width of 138 ± 54 nm.

For FSPS processing, the same SPS technique was used to pre-sinter five 20 g compacts to 70 – 73 % relative density; by processing at 823 K for 30 s under 50 MPa pressure. The resulting compacts were roughly 20 mm in diameter and 12 mm in height. This pre-sintering step ensured that the samples were able to withstand the minimum applied force of 5 kN required to make good electrical contact during FSPS. This step could be replaced with a cold pressing step; or, with appropriate equipment and process design, could be eliminated altogether.

To perform FSPS, these samples were placed into the SPS furnace between two 40 mm diameter graphite punches and wrapped in graphite felt to minimise heat loss from the edges and assist in pre-heating. Under constant applied force of 5 kN (nominal pressure of 16MPa) and vacuum (5 Pa) the samples were heated to 723 K (the minimum temperature required for a pyrometer reading), held for 1 min to stabilise and even out the sample temperature, and then flash sintered by discharging for 10 s under peak heating powers of 8, 9, 10, 11 or 12 kW. The power was then shut off and the sample left under the 5 kN load in order to cool quickly in contact with the water-cooled pistons.

Note that the sample temperature is expected to be much higher than the observed pyrometer reading taken from inside the top punch; since the high heating rates encountered during the short FS times lead to the generation of large temperature gradients between the sample and punch. In order to assess the temperature profile more accurately, two more samples were FSPS processed under the maximum peak heating power used (12 kW) with temperature logged using a k-type thermocouple inserted into the middle of the sample. Note that there is a delay in temperature reading (typically < 0.5 s) associated with the reduced thermal conductivity of the thermocouple, due to the electrical insulation of the hot junction. The temperature profiles obtained from both samples were in close agreement. Temperatures of up to 1343 K and heating rates up to 2660 K min^{-1} were recorded. The power output, sample temperature and deformation rate data recorded under a peak heating power of 12 kW can be seen in supplementary figure A.

The final densities of the flash sintered samples were measured from ≈ 1 cm^2 pieces cut from the centres of the samples using the Archimedes method.

3.1 Results and Discussion

Figure 1 shows the average grain aspect ratio and density of the FSPS processed samples, along with the average deformation rate during the 10 s flash discharge as a function of the peak applied heating power. It can be seen that near-theoretical density (above 7.6 g cm^{-3}) was achieved under

the highest applied powers, with deformation rates up to 3.6 s^{-1}. This is particularly notable considering the short processing times.

With increasing peak applied power, the deformation rate first increased and then plateaued at around 10 to 11 kW. At peak heating powers below 10 kW, the samples were observed to be cracked across their full width (see supplementary figure B) and consequently exhibited much lower densities. Such defects were not observed at 10 kW and above, suggesting that the samples had plastically deformed, while still achieving near-theoretical densities. The plateau in deformation rate is therefore most likely due to the increase in sample cross section in contact with the punches under the high plastic deformation rates generated at these discharge powers. This increased sample cross section led to an overall decrease in pressure and current density through the sample and therefore a decrease in deformation rate. However, the deformation rate rapidly increased again at the maximum peak heating power of 12 kW; leading to the maximum observed height reduction of 54 %. This sudden increase in deformation rate was due to the increased temperatures; and is accompanied by a sudden increase in the average grain aspect ratio.

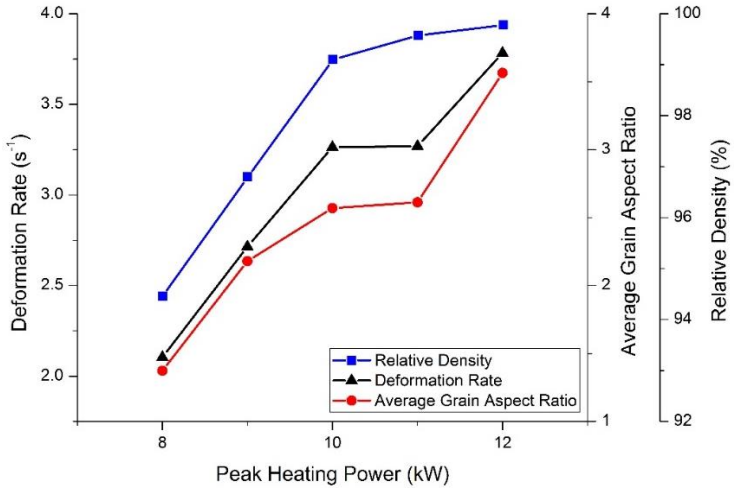

Figure 1. Sample deformation rate, relative density and average grain aspect ratio as a function of peak heating power observed during FSPS.

In all of the samples, regions of fine, equiaxed grains and regions of aligned, plate-like grains were observed; examples of which are shown in **figure 2**. **Figure 3** is a histogram showing the distribution of grain aspect ratio in each sample. All of the samples, except the standard SPS sample and the lowest peak heating power sample (8 kW), exhibited a bi-modal distribution in aspect ratio; relating to the mixture of some volume fraction of equiaxed grains and some volume fraction of plate-like grains. With increasing power, the grain aspect ratio distribution broadened; reflecting the increasing volume fraction of plate-like grains and the increasing average grain aspect ratio. Where the plateau in deformation rate was observed for the 10 and 11 kW samples, the distributions of grain aspect ratio are very similar. Moreover, where the jump in deformation rate at 12 kW was observed, there is a corresponding broadening of the distribution; indicating the onset of enhanced anisotropic grain growth. Under conventional hot deformation processing, it has been shown that the preferential elongation of grains occurs through an interface-controlled solution-precipitation creep process; which is enhanced through the formation of a liquid grain boundary phase at around 670 ^{o}C [23, 24]. If this is also the dominant mechanism operating under the FSPS processing

conditions, then the jump in deformation rate and enhanced anisotropic grain growth observed under the highest 12 kW heating powers may be explained by the melting of the grain boundary phase. Further multiscale microstructural investigations will be required in order to confirm the dominant grain growth and deformation mechanism and the factors which influence the degree of crystallographic alignment.

An encouraging feature of these microstructures is that, while grain growth was observed, the average grain width remained nanoscale; with average widths increasing from 140 nm to 221 nm as the power was increased from 8 kW to 12 kW.

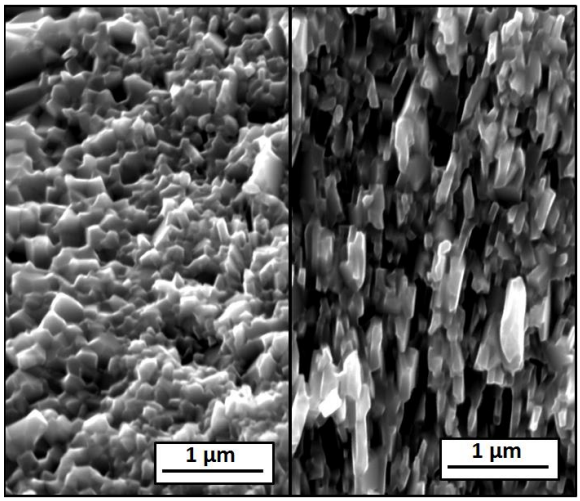

Figure 2. The FSPS-processed sample discharged for 10 s under a peak heating power of 10 kW. The pressing direction is horizontal with respect to both images. Examples of: (left) fine, unaligned, equiaxed grains; and (right) plate-like grains exhibiting a high degree of alignment.

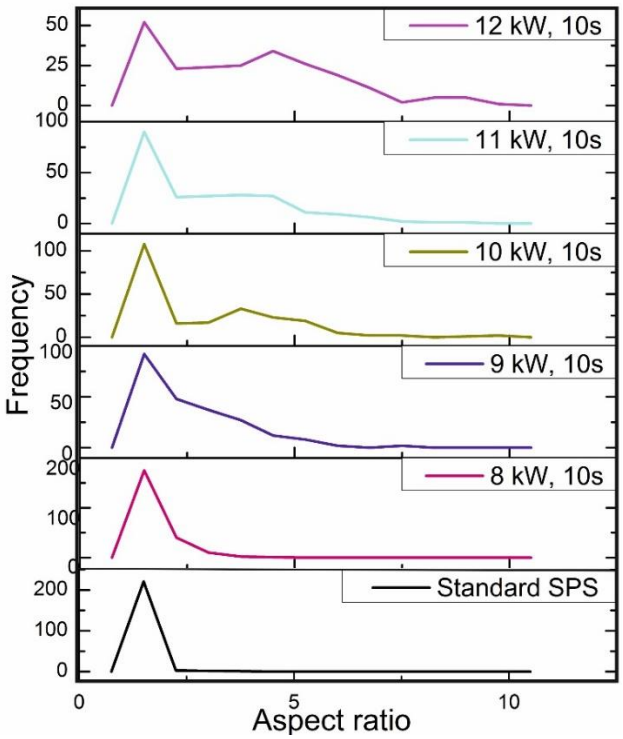

Figure 3. Histograms showing the distribution of grain aspect ratio for the FSPS-processed samples and standard SPS-processed sample.

The magnetic properties of the samples were measured using a LakeShore 7000 Series vibrating sample magnetometer (VSM). The magnetic properties quoted have not been corrected for the self-demagnetisation that occurs in open-loop measurement systems. A small cube (5x5x5 mm) was cut from the centre of the samples and measured parallel and perpendicular to the pressing direction (in the 'easy' and 'hard' magnetisation directions, respectively). The demagnetisation quadrant of the hysteresis loops for these samples is shown in **figure 4**. The standard SPS magnet exhibited almost identical demagnetisation loops in the parallel and perpendicular directions, which signifies the isotropic nature of the sintered compact. The flash sintering method, however, produced materials with anisotropic properties. The degree of magnetic anisotropy is shown in **figure 4** (bottom) and was calculated using the formula:

$$\text{Magnetic Anisotropy} = \frac{B_{r\parallel} - B_{r\perp}}{B_{r\parallel}} \qquad \text{Equation (1)}$$

Where $B_{r\parallel}$ is the remanent flux density parallel to the easy axis of magnetisation, and $B_{r\perp}$ is the remanent flux density parallel to the hard direction of magnetisation. A value of 1 indicates 100 % magnetic alignment and a value of 0 indicates that the sample is completely magnetically isotropic. For the samples processed at 8-11 kW, the degree of anisotropy was quite low (<0.22). However, at 12 kW power there was a significant difference between the demagnetisation loops in the two magnetisation directions, producing a magnetic anisotropy of 0.50. This sudden increase in magnetic anisotropy coincided with the high deformation rate and average grain aspect ratio previously observed in **figure 1**. Although the remanence of this specimen (~0.85 T) was lower than that of conventionally sintered Nd-Fe-B magnets (~1.2 T) [2], it is worth noting that the coercivity value exceeded the measurable limit of the VSM (1600 kAm^{-1}); a value which is much higher than commercial sintered Nd-Fe-B (~1050 kAm^{-1}) [2]. This is due to the the nanoscale characteristics of the $Nd_2Fe_{14}B$ grains observed in the FSPS processed material. With further optimisation of the flash sintering process, as well as the inclusion of a post-sintering annealing step, it will be possible to increase the grain size; potentially leading to an increase in remanence at the expense of coercivity, allowing the magnetic properties to be tailored. The volume fraction of plate-like grains may also be increased to improve the magnetic remanence, following further detailed studies into the effect of FSPS processing parameters on the evolution of microstructure and magnetic properties.

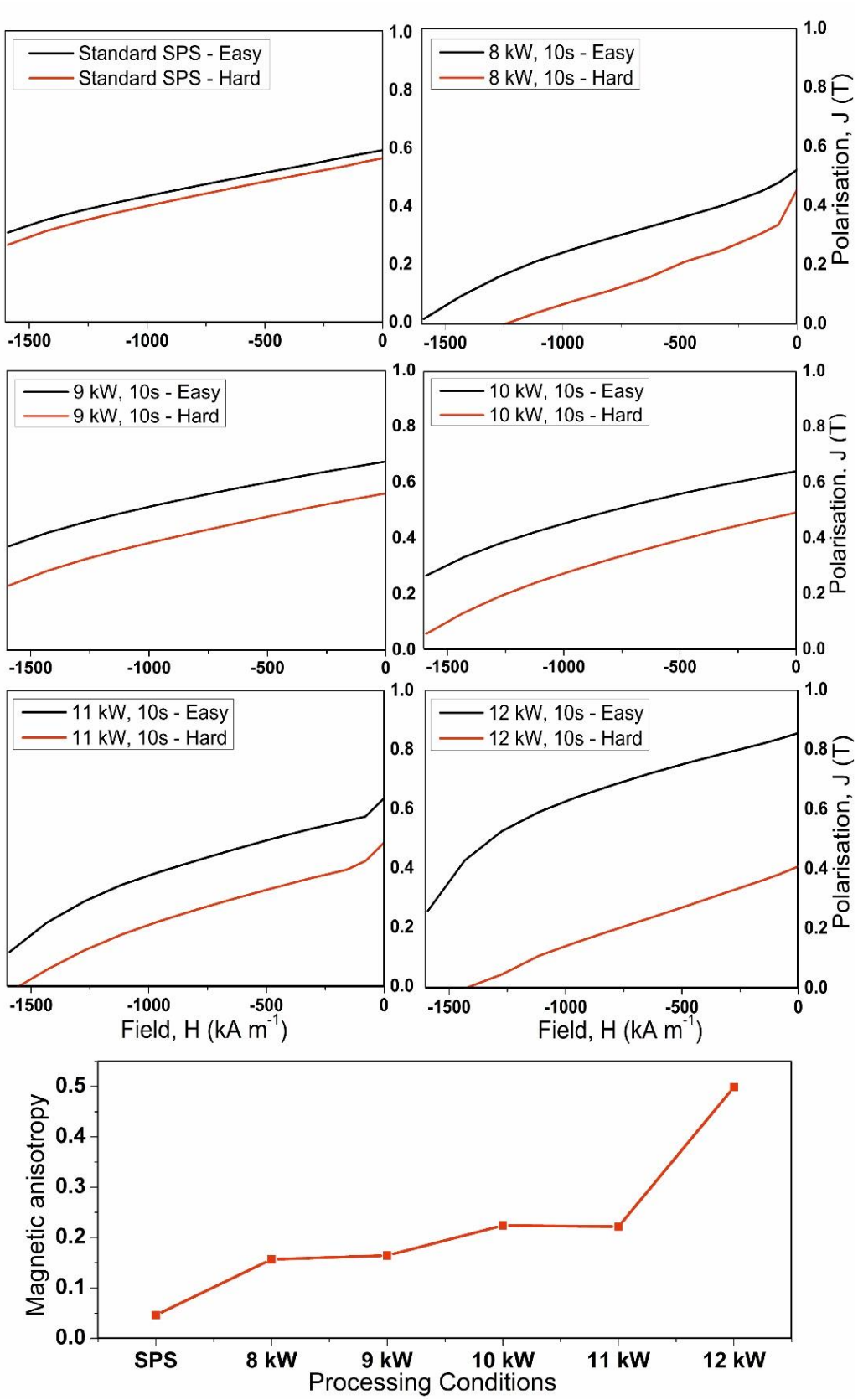

Figure 4. Demagnetisation curves for the easy and hard directions of FSPS samples discharged for 10 s under different heating powers, as compared to the sample densified by standard SPS; and magnetic anisotropy (as calculated from equation 1.0) of the FSPS and SPS samples.

4.1 Conclusions

In summary, Flash Sintering has been performed on Nd-Fe-B type permanent magnetic powders using a Spark Plasma Sintering furnace. Using a combination of a 30 s SPS pre-sintering step, and a 10 s Flash-SPS step, near theoretical densities were achieved. The high deformation rates (<3.6 s^{-1}) produced during FSPS yield regions of aligned, nanoscale, plate-like grains in all of the samples. Consequently, an increased magnetic anisotropy was observed in the FSPS materials compared to a sample consolidated using optimised standard SPS processing. Under the highest FSPS discharge power investigated, a sharp increase in the deformation rate (to 3.6 s^{-1}), average grain aspect ratio (<11) and anisotropy in magnetic properties (0.5) was seen; which was produced by anisotropic grain growth and consequent improved grain alignment during deformation. The magnetic properties of this sample were close to those reported for conventional hot-deformed magnets; and in particular, exhibited enhanced coercivity due to the retention of a nanoscale microstructure. For a preliminary study into a new and not yet optimised processing technique; this is a very encouraging result and further investigations are underway.

Acknowledgements: Research supported by EU-FP7 *MAG-DRIVE* project (No. 605348) [http://www.mag-drive-fp7.eu/]

References

[1] M. Tokunaga, Y. Nozawa, K. Iwasaki, S. Tanigawa, H. Harada, Journal of Magnetism and Magnetic Materials, 80 (1989) 80-87.
[2] R.W. Lee, E.G. Brewer, N. Schaffel, Magnetics, IEEE Transactions on, 21 (1985) 1958-1963.
[3] Y. Nozawa, K. Iwasaki, S. Tanigawa, M. Tokunaga, H. Harada, Journal of Applied Physics, 64 (1988) 5285-5289.
[4] J. Song, M. Yue, J. Zuo, Z. Zhang, W. Liu, D. Zhang, J. Zhang, Z. Guo, W. Li, Journal of Rare Earths, 31 (2013) 674-678.
[5] W. Mo, L. Zhang, A. Shan, L. Cao, J. Wu, M. Komuro, Intermetallics, 15 (2007) 1483-1488.
[6] T. Saito, T. Takeuchi, H. Kageyama, Production of Nd-Fe-B magnets by spark plasma sintering, in: S. Miyake (Ed.) Novel Materials Processing by Advanced Electromagnetic Energy Sources, Elsevier Science Ltd, Oxford, 2005, pp. 297-300.
[7] K. Suresh, T. Ohkubo, Y.K. Takahashi, K. Oh-ishi, R. Gopalan, K. Hono, T. Nishiuchi, N. Nozawa, S. Hirosawa, Journal of Magnetism and Magnetic Materials, 321 (2009) 3681-3686.
[8] G.P. Wang, W.Q. Liu, Y.L. Huang, S.C. Ma, Z.C. Zhong, Journal of Magnetism and Magnetic Materials, 349 (2014) 1-4.
[9] M. Yue, A.L. Cao, G.P. Wang, W.Q. Liu, D.T. Zhang, J.X. Zhang, Y.P. Luo, X.Y. Zhang, Y.M. Li, Journal of Iron and Steel Research, International, 13, Supplement 1 (2006) 312-315.
[10] Y. Ma, Y. Liu, J. Li, H. Du, J. Gao, Journal of Rare Earths, 27 (2009) 1023-1026.
[11] Y.H. Hou, Y.L. Huang, Z.W. Liu, D.C. Zeng, S.C. Ma, Z.C. Zhong, Materials Science and Engineering: B, 178 (2013) 990-997.
[12] X.-q. Li, L. Li, K. Hu, Z.-c. Chen, S.-g. Qu, C. Yang, Transactions of Nonferrous Metals Society of China, 24 (2014) 3142-3151.
[13] Z. Hu, L. Chu, J. Li, Y. Liu, Journal of Rare Earths, 29 (2011) 660-663.
[14] Z. Hu, H. Qu, J. Zhao, C. Luo, J. Li, Y. Liu, Journal of Rare Earths, 30 (2012) 1112-1115.

[15] M. Cologna, B. Rashkova, R. Raj, Journal of the American Ceramic Society, 93 (2010) 3556-3559.
[16] N. Shomrat, S. Baltianski, C.A. Randall, Y. Tsur, Journal of the European Ceramic Society, 35 (2015) 2209-2213.
[17] A. Gaur, V.M. Sglavo, Journal of the European Ceramic Society, 34 (2014) 2391-2400.
[18] A.L.G. Prette, M. Cologna, V. Sglavo, R. Raj, Journal of Power Sources, 196 (2011) 2061-2065.
[19] E. Zapata-Solvas, S. Bonilla, P.R. Wilshaw, R.I. Todd, Journal of the European Ceramic Society, 33 (2013) 2811-2816.
[20] R. Muccillo, E.N.S. Muccillo, Journal of the European Ceramic Society, 34 (2014) 915-923.
[21] S.K. Jha, R. Raj, Journal of the American Ceramic Society, 97 (2014) 527-534.
[22] S. Grasso, T. Saunders, H. Porwal, O. Cedillos-Barraza, D.D. Jayaseelan, W.E. Lee, M.J. Reece, Journal of the American Ceramic Society, 97 (2014) 2405-2408.
[23] W. Grünberger, D. Hinz, A. Kirchner, K.H. Müller, L. Schultz, Journal of Alloys and Compounds, 257 (1997) 293-301.
[24] A. Kirchner, W. Grünberger, O. Gutfleisch, V. Neu, K.-H. Müller, L. Schultz, Journal of Physics D: Applied Physics, 31 (1998) 1660.

Supplementary Material

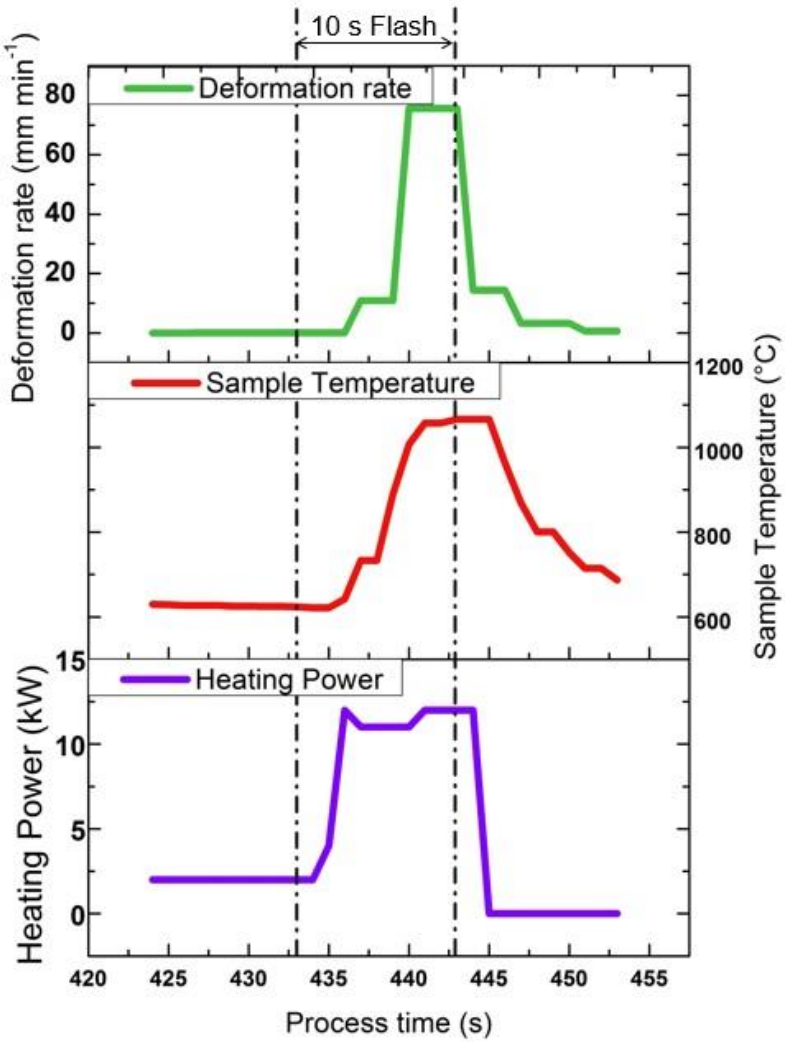

Figure A. Applied heating power, sample temperature (as measured with a thermocouple inserted into the sample) and deformation rates achieved during the 10 s flash.

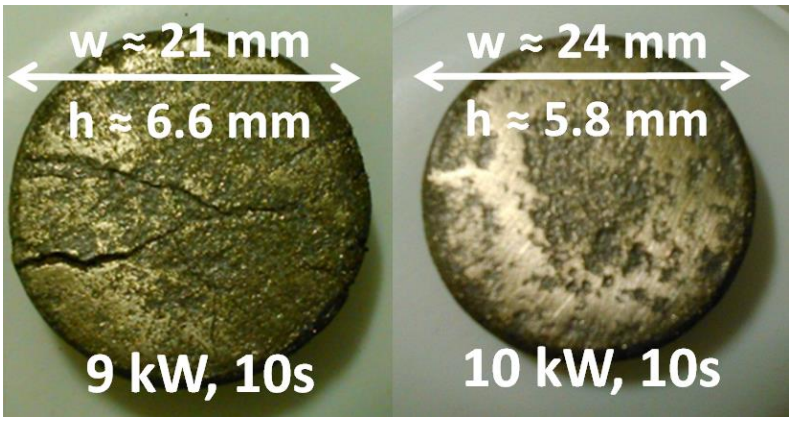

Figure B. (Left) FSPS sample discharged under 9 kW peak heating power, exhibiting cracks ; and (right) the sample discharged under 10 kW peak heating power, which exhibits no cracking.